

# Photoelastic characterization of residual stress in GaAs-wafers

H.D. Geiler<sup>a,\*</sup>, H. Karge<sup>a</sup>, M. Wagner<sup>a</sup>, St. Eichler<sup>b</sup>, M. Jurisch<sup>b</sup>,  
U. Kretzer<sup>b</sup>, M. Scheffer-Czygan<sup>b</sup>

<sup>a</sup>JenaWave GmbH, Konrad-Zuse-Street 5, D-07745 Jena, Germany

<sup>b</sup>Freiberger Compound Materials, Am Junger Löwe Schacht 5, D-95099 Freiberg, Germany

Available online 20 February 2006

## Abstract

Residual stress in GaAs-wafers was investigated on different length scales by rapid full wafer imaging and by microscopic imaging of dislocation cells, using photoelastic homodyne techniques. These non-contact and non-destructive defect and stress imaging methods will be described in detail. In connection with in situ calibration of the photoelastic SIRD<sup>TM</sup> measurement system absolute shear stress values can be extracted. Local stress fields imaged in  $\mu\text{m}$ -scale by the photoelastic instrument SIREX<sup>TM</sup> show the defect arrangement in cell patterns and allow to characterize the local stress enhancement. The advantages and limits of the vertically integrated photoelasticity measurement employed in both systems will be discussed.

© 2006 Elsevier Ltd. All rights reserved.

PACS: 07.60-j; 42.62Cf; 61.72Hh; 78.20Hp; 81.05Ea

Keywords: Stress imaging; Photoelasticity; GaAs crystal; Defect monitoring; Nondestructive evaluation

## 1. Introduction

Recent progress in crystal growth technologies of GaAs both by liquid encapsulated Czochralski (LEC) and vertical gradient freeze (VGF) technique in connection with post-growth thermal treatment allows the preparation of wafers with tailored device specific properties [1–3]. In single crystalline compound semiconductors, the dislocations, which are generated during crystal growth by thermoplastic relaxation of thermal stress fields and possibly modified during subsequent heat treatment, are

the source of local and global residual stress in the wafers manufactured from these crystals. Size and distribution of these lattice incompatibilities and their resulting residual stress fields influence the geometrical, electrical and possibly fracture properties of these wafers [4]. In addition, residual stress fields interact with native and intrinsic defects in the material resulting in inhomogeneities with influence on device properties and their reliability [1]. Like in manufacturing of upgraded silicon-wafers the control of residual stress by rapid nondestructive evaluation methods should be an integral part of quality management in the development of technology as well as in production [5–6]. For nondestructive evaluation of strain and stress fields in semiconductor wafers, different methods

\*Corresponding author. Tel.: +49 3641616748;  
fax: +49 3641616748.

E-mail address: [jenawave@t-online.de](mailto:jenawave@t-online.de) (H.D. Geiler).

like X-ray topography [7] and a variety of photoelastic stress imaging systems based on infrared polariscopes [6–8] are widely used. In the current paper the photoelastic homodyne (PEH) technique is applied for a full wafer-shear stress imaging as well as for local stress analysis in GaAs wafers grown by LEC and VGF technology. This method is characterized by its high sensitivity (0.5 kPa in 150 mm wafers) and short measurement times (3 mi for full wafer imaging). For our investigations the commercial available systems SIRD<sup>TM</sup> (PVA TePla AG) and SIREX<sup>TM</sup> (JenaWave GmbH) were used in connection with a new alternating retarder difference (ARD) method demonstrating the capability of global and local absolute stress imaging in the well-known defect structures of GaAs like glide bands, sliplines, dislocation cells and lineages [7].

## 2. PEH method with ARD

To study the residual stress fields in GaAs-wafers with respect to their global and local distributions in the wafer plane (plain stress approximation) two kinds of infrared polarimeters were used: (a) the rapid scanning infrared transmission polarimeter SIRD<sup>TM</sup> [5] supplies full wafer shear stress images in polar coordinates with a lateral resolution of 100  $\mu\text{m}$  and (b) microscopic imaging in regions of 2 mm  $\times$  2 mm extension with a lateral resolution of 1  $\mu\text{m}$  was carried out by the scanning reflection polarimeter SIREX<sup>TM</sup> to investigate the local shear stress fields in  $x$ - $y$ -coordinates. The optical scheme of these systems are shown in Fig. 1. In both systems, a linear polarized laser beam of 1.3  $\mu\text{m}$  wavelength is passing through the wafer. Due to the stress induced birefringence inside the wafer, the electrical field vector is split into two perpendicularly arranged components (ordinary and extraordinary beam), which are related to the principal stress components in the wafer plane  $\sigma_1$  and  $\sigma_2$ , respectively. The different phase velocities of the ordinary and extraordinary beam result in a phase difference  $2\Gamma$  during their propagation through the wafer with the thickness  $d$ . The phase shift  $\Gamma$  is

related to stress by the Wertheim law [9]

$$\Gamma = \frac{\pi d}{\lambda} C_\sigma (\sigma_1 - \sigma_2). \quad (1)$$

If the stress optical constant of the material  $C_\sigma$  is known, the optical determination of  $\Gamma$  allows the absolute measurement of the principal stress difference according to Eq. (1). The phase shift is determined indirectly by recording the depolarization  $D$  (the change of the first Stokes component [5]). In the SIRD system the wafer is scanned through the fixed laser beam by spinning on a rotation-translation stage with edge grabbers. The data are recorded in polar coordinates with the origin in the wafer center and the angular position counterclockwise rotated beginning from the notch. The polarization direction is exactly adjusted collinear to the wafer radius. In contrast to SIRD, the SIREX applies a  $x$ - $y$ -scan with a selectable but during scanning fixed polarization direction. In this geometry the laser light reflected from the wafer backside has to be analyzed for determining the depolarization caused by the birefringence inside the wafer. Hence, twice the wafer thickness has to be introduced in Eq. (1) for  $d$ . The standard depolarization  $D$  is calculated from the photo currents of the polarization components of the transmitted light  $P_\perp$  and  $P_\parallel$  oriented parallel and perpendicular, respectively, to the incident linear polarization vector [5]. The photodiodes of the analyzer act as square-law detectors in video mode for the electromagnetic field strength [10]. For the expected very small perpendicular components  $E_\perp$ , a linear receiver is desired, which can be realized, in the homodyne mode by mixing the signal with a defined elliptical field component [10]. In case of vanishing  $E$ , this field component produces a remaining depolarization  $D_o$  as an instrument constant. The desired local oscillator field is created by the alternating phase shift technique ARD. Let  $\gamma$  be the angle between the local principal stress axis in the wafer and the wafer radius direction. Then, subsequently, an additional phase plate characterized by the alternating phase shift  $\pm\Lambda$  and a very small rotation by the angle  $\rho$  is introduced (alternating retarder). The normalized intensity  $I_\perp$  received in the perpendicular detector channel can be calculated by the Jones matrix formalism [11]

$$D = 2 \frac{I_\perp}{I_\parallel + I_\perp} = 2 \sin^2 \Gamma \sin^2 \Lambda [\sin^2 2(\gamma - \rho) - \sin^2 2\gamma - \sin^2 2\rho] + 2 \sin^2 \Gamma \sin^2 2\gamma + 2 \sin^2 \Lambda \sin^2 2\rho + \sin 2\Lambda \sin 2\rho \sin 2\Gamma \sin 2\gamma. \quad (2)$$

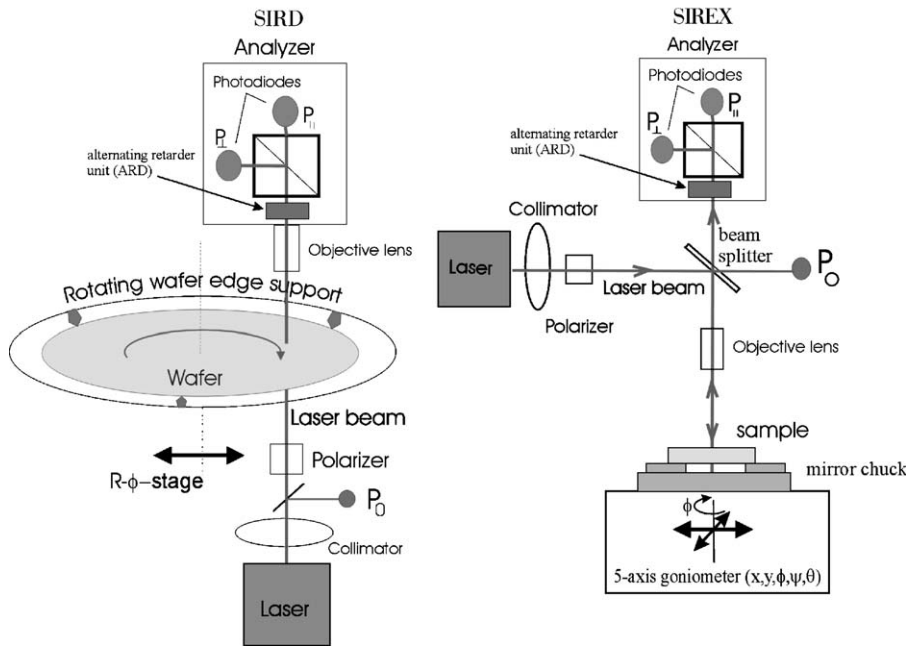


Fig. 1. Optical schemes of the PEH equipments SIRD and SIREX with ARD technology.

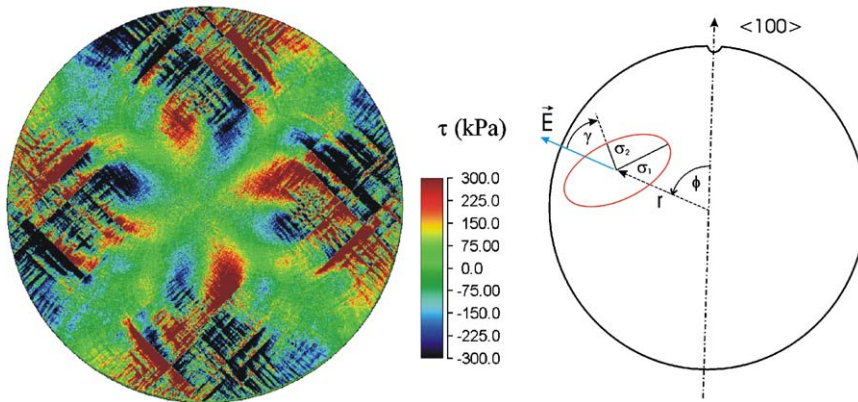


Fig. 2. Shear stress image of a polished LEC GaAs-wafer (left) and the geometry of a local plain stress tensor visualized by an ellipse with the principal stress components  $\sigma_1$  and  $\sigma_2$  in wafer polar coordinates  $r, \phi$ .

The fourth term on the right-hand side of Eq. (2) is linear in  $\sin 2\Gamma$  and can further be linearized for small values of the phase shifts  $\Gamma$  according to  $\sin 2\Gamma \approx 2\Gamma$ . The third term represents the local oscillator field  $D_0$  caused by the retarder without any wafer. The difference of the depolarizations  $D(+\Delta)$  and  $D(-\Delta)$  with the switched phase  $\pm\Lambda$ , respectively, supplies

$$D(+\Lambda) - D(-\Lambda) = \sqrt{2} \times 4\Gamma \sin 2\gamma \sqrt{D_0}, \quad (3)$$

where  $D_0 = 2 \sin^2 \Lambda \sin^2 2\rho$ .

Taking into account the relation between the principal stress components and the shear stress  $\tau$ , the basic equation for the transformation of the difference depolarization image into a shear stress image is obtained:

$$G = \frac{D(+\Lambda) - D(-\Lambda)}{2\sqrt{D_0}} = M\tau = M \frac{\sigma_1 - \sigma_2}{2} \sin(2\gamma), \quad (4)$$

with the wafer module  $M = \sqrt{2} 4\pi d / \lambda C_\sigma$ . The so constructed quantity  $G$  is called the shear stress equivalent. The wafer modulus can be taken from a material table or determined experimentally by a

special in situ calibration procedure [9–12]. This calibration is performed inside the SIRD system directly on a GaAs-wafer by applying a defined radial acting force set on the wafer edge and measuring the resulting maximum shear stress equivalent  $G$  in the wafer center [12]. Using the analytical shear stress in the center of a wafer of radius  $R$  and thickness  $d$  [13], the wafer module  $M$  is calculated. The transformed shear stress image in absolute units is defined in the polar coordinate system of the wafer (see Fig. 2). Because of the anisotropy of the GaAs crystal and the resulting anisotropy of the stress optical constant  $C_\sigma$ , different values of the wafer modulus will be found for different force directions. In case of 150 mm wafers  $M$  varies between 0.28 and  $0.16 \text{ MPa}^{-1}$  with force direction in  $\langle 110 \rangle$  and  $\langle 100 \rangle$ , respectively. For all shear stress images the mean value of  $0.24 \text{ MPa}^{-1}$  determined for 150 mm wafers with  $675 \mu\text{m}$  thickness was used to transform the scales in SI units.

### 3. Shear stress images and distributions of GaAs-wafers: results and discussion

To demonstrate the capabilities of the described PEH method residual stress measurements on 150 mm  $\langle 100 \rangle$  grown semi-insulating GaAs-wafers have been performed, which are cut from LEC and VGF crystals. As an expressive example Fig. 2 shows the full wafer shear stress image of a heavily stressed LEC wafer recorded by SIRD. The quantification by the color scale indicates that the SIRD method allows to determine the sign of the shear stress given in polar coordinates. The main features of the mapping shown are:

- A cross-like area with an apparently vanishing shear stress. This is caused by an inherent property of the photoelastic method. If the radially oriented polarization vector coincides with any direction of principals stresses, i.e. if  $\gamma = 0$  in Fig. 2, no birefringence occurs and therefore no related depolarization is measured.
- Furthermore, a pronounced four fold sequence of positive and negative shear stress in the inner part as well as near the periphery of the wafer is observed with the sequence being of opposite sign in the central and peripheral part. In this region  $\gamma$  is unequal to zero. This leads to the conclusion that compressive and tensile stress rings exist in the wafer. With reference to the

scale gained from an independent elastic calibration experiment, the inner ring is compressive, the outer one tensile.

- In addition, the global stress field of this LEC wafer is dominated by  $\langle 110 \rangle$  oriented glide bands starting at wafer edge regions with maximum Schmid factor of the thermally induced stress [14]. These glide bands are extended up to about the half of wafer radius  $R$  and accompanied by shear stress fields. The wafer center is free from these strong glide bands.

To compress these qualitative results into simple assessable technological parameters, the radial dependence of the maximum shear stress in a ring area of radius  $r$  is calculated. This is done by fitting the azimuthal variation of shear stress at constant  $r$  by  $A \cos(4\phi - \gamma_G)$  with  $A$  as the maximum stress at  $r$  and the offset angle  $\gamma_G$  of the local principal stress direction. As an example the radial distribution of the difference of the principal stress components (twice the maximum shear stress) measured on a sequence of VGF-grown wafers taken from different positions in the ingot is represented in Fig. 3. Compressive as well as tensile stress rings are found for wafers 22 and 27 with maximum stress values around 50 kPa. In contrast, wafer 37 exhibits tensile stress only across the whole wafer area.

As a measure to characterize the imaged stress fields quantitatively, a shear stress distribution function of the image can be calculated and the moments of this image can be related to quality criteria. Fig. 4 displays the stress distribution

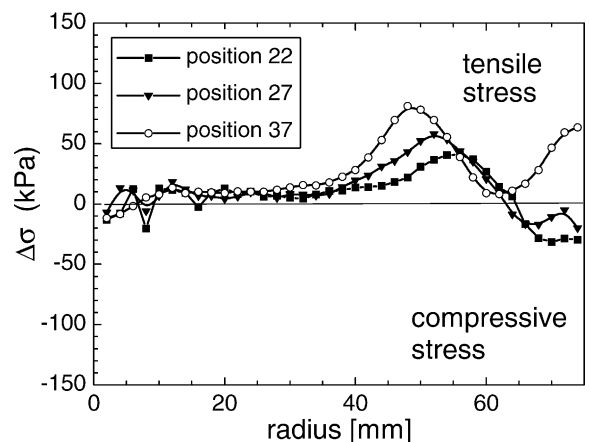


Fig. 3. Difference of the principal stress components ( $\sigma_1 - \sigma_2$ ) versus radius of 3 VGF-grown GaAs-wafers sliced at different positions of the ingot.

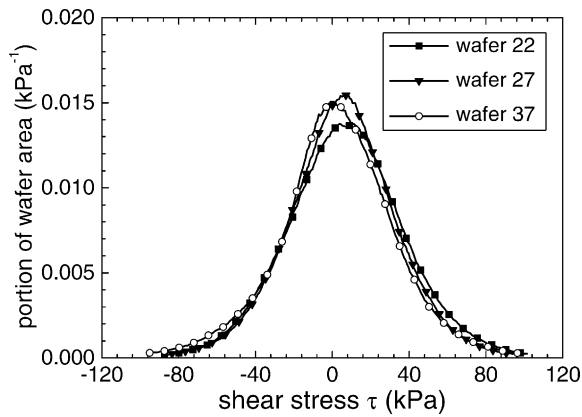


Fig. 4. Shear stress distribution of the three VGF-wafers analyzed in Fig. 3.

functions of the same set of VGF wafers used for analysis in Fig. 3. For standard wafers these histograms can be fitted by Lorentz curves supplying the full-width at half-maximum (FMHW) as a parameter to evaluate the stress content of the wafer. As can be seen from Fig. 4 the FMHW is about 100 kPa. This is a typical value for state of art VGF-GaAs wafers. Due to stronger glide bands the FWHM observed in LEC wafer can be significantly higher.

To assess local stress in greater detail, the microscopic shear stress distribution has been investigated by high-resolution SIREX mapping. As an example, the mapping of the shear stress field of a 4 mm × 6 mm central area of a VGF wafer is compared with the dislocation etch pit mapping of the same area taken by DC Normarsky microscopy in Fig. 5. A cellular arrangement of dislocation bundles revealed by small stress monopoles can be clearly recognized. A few dislocations can be found inside the cells but most of them are concentrated in the cell walls. The corresponding shear stress fields extend over characteristic lengths of about 10–50 μm. The cell size is about 2 mm most. Note that the etch pits mark the emerging points of dislocations on the surface, whereas the shear stress image is the photoelastic integration over the wafer thickness. Therefore, the etch pit pattern and the cell walls or monopoles are not completely congruent.

Despite high sensitivity of 0.5 kPa some restrictions have to be taken into account. The probing laser beam is perpendicular to the wafer surface. Therefore, only stress components in the wafer plane can be detected and, in addition, stress values calculated by Eq. (4) have to be interpreted as vertically integrated ones (integrating photoelasticity). At present, the rapid

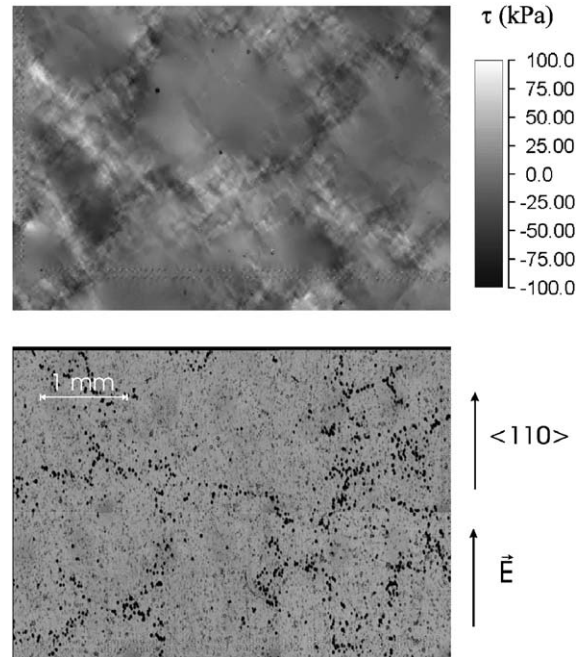


Fig. 5. Microscopic shear stress image of the cell structure of a VGF-grown GaAs-wafer gained by SIREX (upper part) compared with the dislocation etch pit mapping (lower part). The polarization direction of the incident light is parallel  $\langle 110 \rangle$ .

imaging technique SIRD supplies shear stress values only but offers the possibility of a second data record with a changed angle of polarization in each point. This would make it possible to extract the shear stress as well as the difference of the principal stress components separately. Furthermore, as already mentioned above, no birefringence is observed if the polarization vector coincides with a direction of principal stresses.

Local microscopic measurements by the SIREX system can be performed with two or more distinct polarization angles, which allows to determine separately the phase difference  $\Gamma$  and the inclination angle  $\gamma$  of the principal stress direction in Cartesian coordinates.

Measurements by PEH techniques are possible also in case of very small transmission down to  $10^{-4}$ . Hence, stress determination in wafers with high conductivity up to  $6 \times 10^{-3} \Omega \text{cm}$  can be realized without problems.

#### 4. Summary

Rapid scanning photoelastic techniques as used in the SIRD are indispensable nondestructive evaluation methods for process control both on monitor

and product wafers. Quality management and defect monitoring can be done by combining the rapid overview gained by SIRD with the detailed analysis realized by SIREX. The sensitivity of the PEH principle applied in both instruments allows the monitoring of complex defect structures in GaAs not only during wafer manufacturing but also in subsequent process steps of device production. The information content of full shear stress wafer mappings can be compressed into two sets of parameters characterizing maximum global and mean local stress. These parameters can be used as measures to optimize crystal growth and wafering technologies.

## References

- [1] Fornari R. Mater. Sci. Eng. 1991;B9:9–18.
- [2] Jurisch M, Börner F, Bünger T, Eichler S, Flade T, Kretzer U, et al. J. Cryst. Growth 2005;275:283.
- [3] Seidl A, Eichler S, Flade T, Jurisch M, Köhler A, Kretzer U, et al. J. Cryst. Growth 2001;225:561.
- [4] Sumino K. Mechanical behaviour of semiconductors. In: Moss TS, Mahajan S, editors. Handbook of semiconductors, vol.3. New York: Elsevier; 1994. p. 101.
- [5] Geiler HD, Wagner M, Karge H, Paulsen M, Schmolke R. Mat. Sci. Semicon. Proc. 2003;5:445–55.
- [6] Geiler HD, Karge H, Wagner M, Ehlert A, Daub E, Messmann K. Mater. Sci. Eng. 2002;B91–92:46.
- [7] Matsui J. Appl. Surf. Sci. 1991;50:1–8.
- [8] Yamada M. Rev. Sci. Instrum. 1993;64:1815–21.
- [9] Dally JW, Riley WF. Experimental stress analysis. New York: McGraw-Hill; 1991. p.424.
- [10] Yu FTS, Khoo I-C. Principles of Optical Engineering. New York: J.Wiley; 1990. p.98.
- [11] Theocaris PS, Gdoutos EE. *Matrix theory of photoelasticity*. Springer Series in Optical Science, vol.11. Berlin: Springer; 1979. p.34.
- [12] Durelli AJ, Riley WF. Introduction to photomechanics. Englewood Cliff: Prentice-Hall Inc.; 1965. p.66.
- [13] Sokolnikoff IS. Mathematical Theory of Elasticity. New York: Mc.Graw Hill; 1956. p.283.
- [14] Bentini G, Corraera L, Donolato C. J. Appl. Phys. 1984;56:2922.